Appl. Phys. A (2014) 117:307–311
DOI 10.1007/s00339-014-8265-y

Applied Physics A
Materials Science & Processing

Optical nanolithography with λ/15 resolution using bowtie aperture array

Xiaolei Wen · Luis M. Traverso · Pornsak Srisungsitthisunti · Xianfan Xu · Euclid E. Moon

Received: 23 October 2013 / Accepted: 16 January 2014 / Published online: 30 January 2014

Abstract We report optical parallel nanolithography using bowtie apertures with the help of the interferometric-spatial-phase-imaging (ISPI) technique. The ISPI system can detect and control the distance between the bowtie aperture, and photoresist with a resolution of sub-nanometer level. It overcomes the difficulties brought by the light divergence of bowtie apertures. Parallel nanolithography with feature size of 22 ± 5 nm is achieved. This technique combines high resolution, parallel throughput, and low cost, which is promising for practical applications.

1 Introduction

With the development of nanoscale science, nanofabrication technique needs to be continuously improved [1]. Higher resolution and throughput, lower cost, and simplification of system configuration are always the targets to pursue. Among various types of nanofabrication methods, such as electron beam lithography, nanoimprint lithography [2], dip-pen lithography [3] and laser direct writing [4], near-field optical lithography using metallic nano-apertures or antennas is a promising technique due to its capacity of sub-diffraction resolution, cost effective, and possibility of parallel operation. In this type of lithography, sharp-ridged apertures in metal, such as bowtie, C- and H-shaped apertures and plasmonic lenses are important structures as the optical focusing element due to its capability of producing high confined light spots beyond the diffraction limit with enhanced intensity in the near-field region [5–10]. However, the transmitted light of the aperture is subjected to strong divergence. The light emerging from the exit plane is only collimated within tens of nanometers, beyond which it diverges quickly and its intensity decreases significantly [11, 12]. Therefore, a precise distance control between the aperture and the recording material (i.e., the photoresist) is required to achieve stable and repeatable sub-diffraction lithography patterns [6, 10, 13].

In this work, we combine a high precision dynamic gap detection system named interferometric-spatial-phase-imaging (ISPI), with a bowtie aperture-based nanolithography system to realize high quality parallel nanolithography. In this technique, substrates with photoresist are scanned and exposed by light spots focused by bowtie apertures fabricated in the Cr film-covered mask. Meanwhile, the ISPI system is used to measure the gap between the mask and the substrate in real time. These two systems work simultaneously due to different light incident geometry. We demonstrate nanolithography with different scanning speed and working distance under the control of the ISPI system. A 5 × 5 parallel nanolithography with a feature line width of about 22 nm is achieved with optimal lithography parameters.

X. Wen · L. M. Traverso · P. Srisungsitthisunti · X. Xu (✉)
School of Mechanical Engineering and Birck Nanotechnology Center, Purdue University, West Lafayette, IN 47907, USA
e-mail: xxu@ecn.purdue.edu

X. Wen
Department of Optics and Optical Engineering, The University of Science and Technology of China, Hefei 230026, Anhui, China

Present Address:
P. Srisungsitthisunti
Production Engineering Department, King Mongkut's University of Technology North Bangkok, Bangkok 10800, Thailand

E. E. Moon
Department of Electrical Engineering and Computer Science, Massachusetts Institute of Technology, Cambridge, MA 02139, USA

2 Interferometric-spatial-phase-imaging (ISPI)

The ISPI system is implemented to detect the distance between the mask and the substrate, which provides a way for fine alignment and gap control during the lithography process [14]. The gap detection is based on analysis of phase and frequency information of the interference fringes produced by the ISPI gratings [15–17]. As Figs. 1 and 2c, d show, the ISPI gratings consist of a pair of two-dimensional checkerboards, each of which has an overall size of 280 × 20 μm. The checkerboard is composed of periodically arranged squares, whose size and interval are uniform along the *y*-direction but chirped along the *x*-direction. The two adjacent checkerboards are chirped in opposite directions. The incident beam is in the *y*–*z* plane, and the *y*-periodicity of the checkerboard is designed to diffract the beam back to the ISPI scope. The chirped *x*-periodicity is used to produce diffraction beams with a sweep of angles in *x*–*z* plane. The beams further interfere with each other and create a set of fringes on the imaging plane of the ISPI scope. The position and number of the fringes are sensitive to the gap between the mask and substrate. By analyzing the fringes from the adjacent two checkerboards, we can obtain the frequency and phase shift information, which is used to derive the gap value.

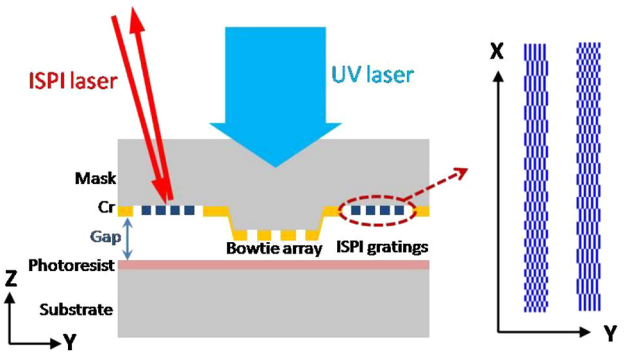

Fig. 1 Schematic diagram of the nanolithography setup. *Inset* is the sketch of ISPI gratings

With use of ISPI frequency gapping, we achieved a parallelism within 0.03 mrad. That means over a 200 × 200 μm^2 area, the gap difference is smaller than 6 nm. On the other hand, the phase gapping is not affected by the Fabry–Perot effect, which is more reliable and accurate than frequency gapping. From calibration, the

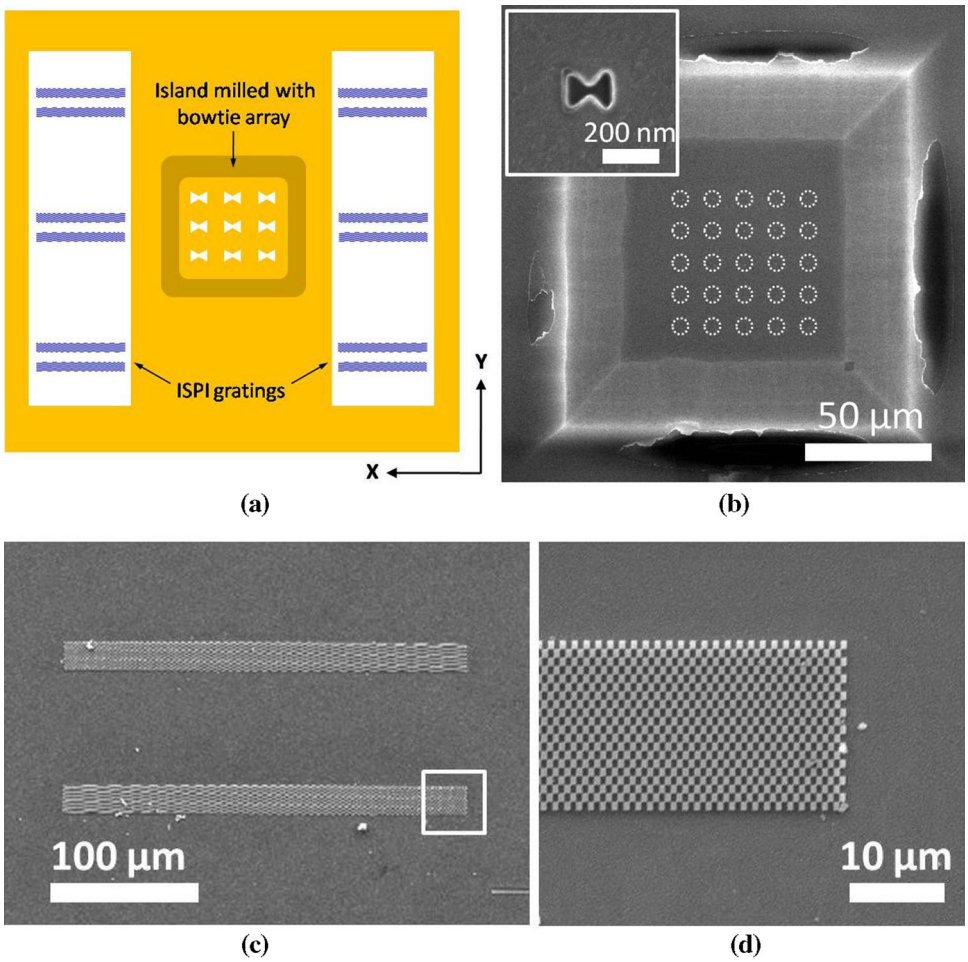

Fig. 2 **a** Sketch of the mask used for the nanolithography, **b** SEM image of the island milled with a 5 × 5 bowtie array (the bowties are marked by *white circles*). *Inset* is a zoom-in image of a bowtie aperture. **c** SEM image of ISPI gratings, **d** zoom-in image of the square area in (**c**)

sensitivity of phase gapping is found to be smaller than 0.5 nm based on our signal detection system.

3 Experimental setup

The experimental setup of near-field nanolithography is built in a semi-closed glove box to reduce contamination. It is composed of gap detection system, ISPI, and the lithography exposure system (Fig. 1). The ISPI system is mounted at an oblique angle so that it does not interfere with the normal-incident exposure beam. The ISPI scope with a 660-nm-wavelength fiber laser is fixed to a six-axis control stage, which can adjust the scope and laser to capture the ISPI images reflected from gratings on the mask. The position and orientation of ISPI scope are aligned carefully for an accurate detection.

A frequency-tripled diode-pumped solid-state UV laser (wavelength 355 nm, pulse width ~25 ns, repetition rate 30 kHz) is utilized as an exposure source for our lithography. The mask is held on a piezo-electric stage which can change its tip–tilt angle for alignment with respect to the substrate. The mask structure is shown in Fig. 2a. We use a piece of 0.5″ square quartz, covered by a 70-nm-thick Cr layer. On the sides of the mask, several sets of ISPI gratings were fabricated by electron beam lithography—EBL. In the center of the mask, there are islands with bowtie arrays fabricated on the top (Fig. 2b). The island is used to reduce the contact area between the mask and the photoresist surfaces, thus to reduce the possibility of contamination and friction. The bowties with outline dimension of 190 × 190 nm are milled by FIB.

Shipley S1805 photoresist was spun on a quartz substrate at 4,500 rpm giving a thickness of 400 nm. The substrate is held on another 5-axis piezo-electric stage which can move in x, y and z directions with a resolution of 0.4 nm and also adjust the tip–tilt angle for alignment. Development was performed using a standard mix of 351 developer and DI water with a ratio of 1:3 for 7 s.

4 Results and discussion

Static tests were first performed with the bowtie apertures to determine a proper exposure dose for the photoresist S1805 we are using. Figure 3 shows AFM images of spots formed from different exposure time under an incident power density of about 10 mW/cm^2. When the time is more than 2 s, the spot size exceeds 300 nm, which indicates overexposure. Under the time of 2 s, the size and depth of the spot decreases with the exposure time. With the time of 0.2 s, the spot can just be distinguished. The threshold of the photoresist is found to be around 2 mJ/cm^2.

The lithography system was then used to produce line patterns by moving the photoresist relative to the fixed exposing source, i.e., the bowtie apertures. Since the effective working distance of bowtie apertures is only tens

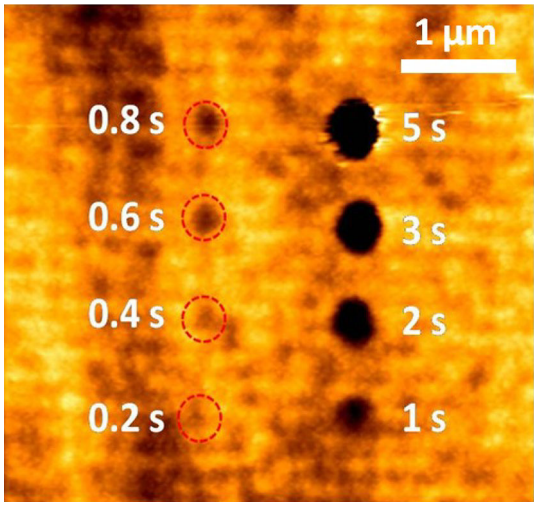

Fig. 3 AFM image of static lithography tests with different exposing time

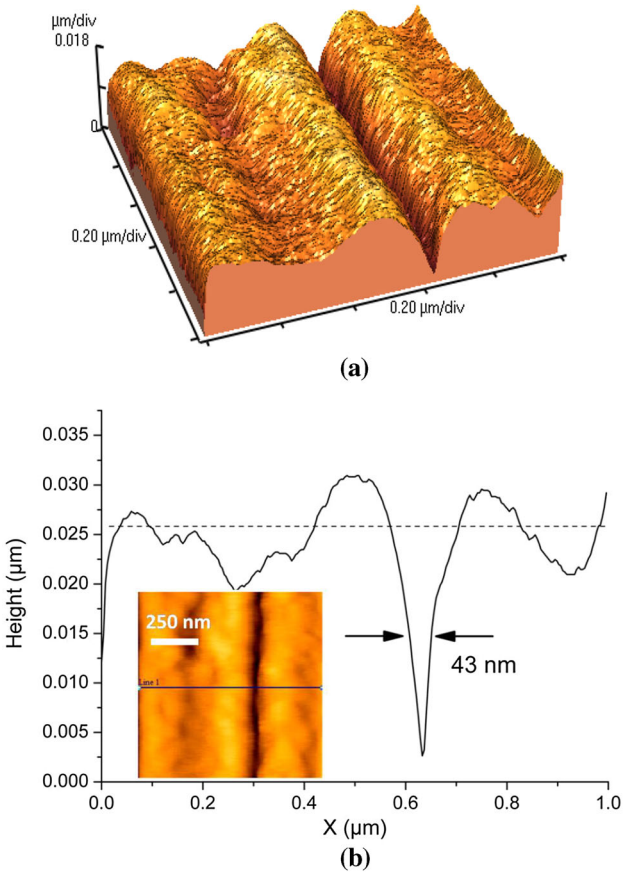

Fig. 4 **a** AFM image of line pattern produced by moving photoresist, **b** a cross-sectional scan of the pattern taken from the position illustrated in the *inset*

of nanometers, there is a strict requirement on the alignment and gap control of the lithography system to obtain high quality sub-diffraction patterns. With the help of ISPI, we can dynamically detect the distance between the mask and substrate for alignment. It also provides a precise control on approaching the photoresist substrate to the bowtie apertures, which not only prevents too much pressure and friction caused by contact, but also ensures that the photoresist surface locates within the sub-50 nm near-field of the bowtie apertures. Figure 4 shows the AFM image of a line pattern produced with a substrate scanning speed of 1 μm/s. The full width at half maximum (FWHM) measured from the cross-sectional scan in Fig. 4b is 43 nm. To investigate the variance in FWHM, we randomly took ten cross-sectional scans on the image and obtained an averaged FWHM ~45 nm with a standard deviation of 6 nm. This line width is much smaller than the overall dimension of the bowtie aperture, but is corresponding to the gap size between the two tips, illustrating light confinement by the bowtie apertures.

By further adjusting the laser power and the gap distance, the smallest line width (FWHM) achieved is ~ 22 ± 5 nm (Fig. 5), which is about 1/15th of the light wavelength that we used for exposure. In this case, a 5 × 5 bowtie array was used as optical focusing elements. With light exposure, 25 patterns were produced simultaneously. As the AFM image is shown in Fig. 5a, these 25 patterns are uniform, due to the alignment provided by the ISPI technique. It is anticipated that further increasing the number of bowtie apertures in the array will significantly increase the efficiency of nanolithography.

5 Conclusion

For near-field bowtie-aperture optical nanolithography, we implemented an ISPI system into the nanolithography system for gap detection and control on the sub-nanometer level. It is shown that with the help of ISPI, we are able to achieve high quality lithography patterns with feature size as small as 22 ± 5 nm. A 5 × 5 bowtie array parallel lithography is also performed, which indicates that this technique has a potential for increasing the efficiency of nanolithography.

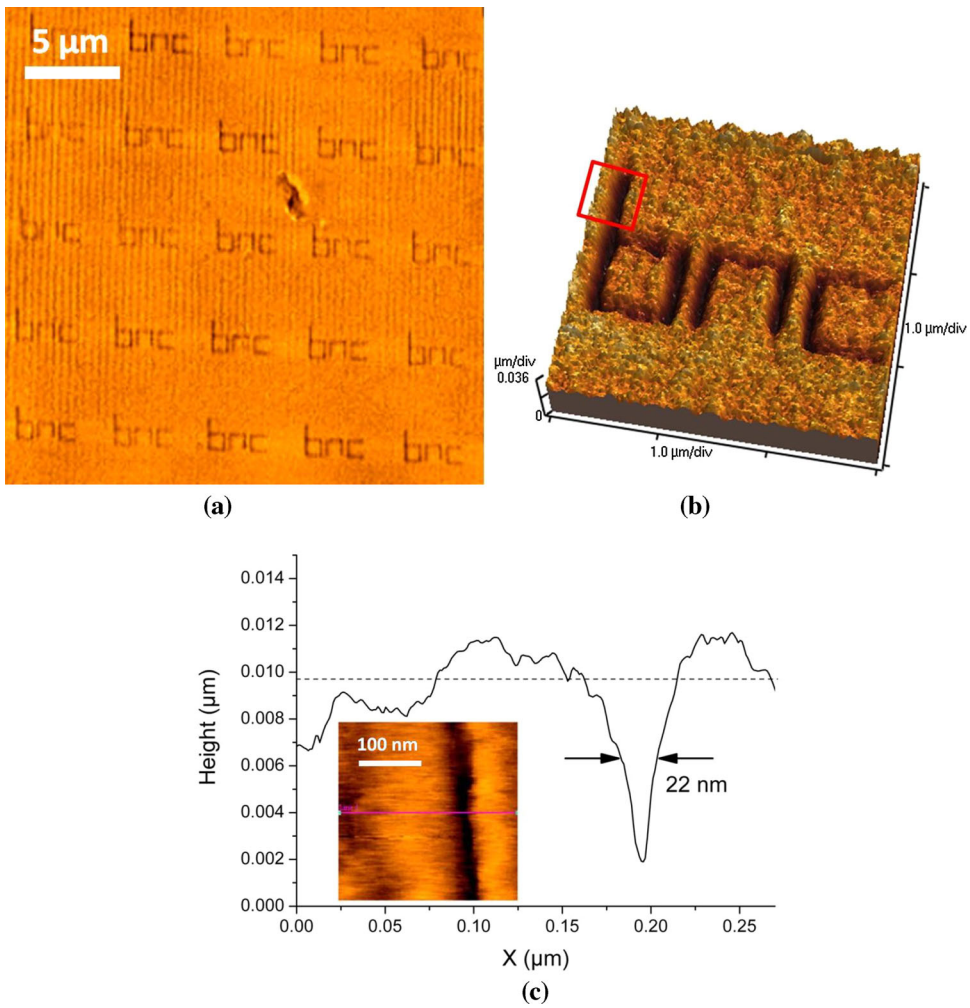

Fig. 5 **a** AFM images of 5 × 5 bowtie array parallel lithography, **b** one unit of the pattern, **c** cross-sectional scan of the pattern taken from the position illustrated in the *inset*. *Inset* is the zoom-in image of the square area in (**b**)

Acknowledgments Support to this work by the Defense Advanced Research Projects Agency (Grant No. N66001-08-1-2037) and the National Science Foundation (Grant No. CMMI-1120577) is gratefully acknowledged. X.W. also acknowledges the support from the National Basic Research Program (973 Program) of China under Grant No. 2013CBA01703 and 2012CB921900.

References

1. Z. Xie, W. Yu, T. Wang, H. Zhang, Y. Fu, H. Liu, F. Li, Z. Lu, Q. Sun, Plasmonics **6**, 565 (2011)
2. S.Y. Chou, P.R. Krauss, P.J. Renstrom, Appl. Phys. Lett. **67**, 3114 (1995)
3. D.L. Wilson, R. Martin, M. Cronin-Golomb, C.A. Mirkin, D.L. Kaplan, Microsc. Microanal. **8**, 1020 (2002)
4. J.I. Mitchell, S.J. Park, C.A. Watson, P. Srisungsitthisunti, C. Tansarawiput, M. Qi, E.A. Stach, C. Yang, X. Xu, Opt. Eng. **50**, 5 (2011)
5. L. Pan, Y. Park, Y. Xiong, E. Ulin-Avila, Y. Wang, L. Zeng, S. Xiong, J. Rho, C. Sun, D.B. Bogy, X. Zhang, Sci. Rep. **1**, 175 (2011)
6. T. Kim, W.S. Lee, H.E. Joe, G. Lim, G.J. Choi, M.G. Gang, S.M. Kang, K.S. Park, B.K. Min, Y.P. Park, N.C. Park, Appl. Phys. Lett. **101**, 161109 (2012)
7. Y. Kim, S. Kim, H. Jung, J.W. Hahn, Proc. SPIE **7637**, 76371F (2010)
8. L. Wang, S.M. Uppuluri, E.X. Jin, X. Xu, Nano Lett. **6**, 361 (2006)
9. S.M.V. Uppuluri, E.C. Kinzel, Y. Li, X. Xu, Opt. Exp. **18**, 7369 (2010)
10. N. Murphy-DuBay, L. Wang, X. Xu, Appl. Phys. A **93**, 881 (2008)
11. E.X. Jin, X. Xu, Jpn. J. Appl. Phys. **43**, 407 (2004)
12. P. Srisungsitthisunti, O.K. Ersoy, X. Xu, Appl. Phys. Lett. **98**, 223106 (2011)
13. W. Srituravanich, L. Pan, Y. Wang, C. Sun, D.B. Bogy, X. Zhang, Nat. Nanotechnol. **3**, 733 (2008)
14. X.L. Wen, L.M. Traverso, P. Srisungsitthisunti, X. Xu, E.E. Moon, J. Vac. Sci. Technol. B **31**, 041601 (2013)
15. E.E. Moon, L. Chen, P.N. Everett, M.K. Mondol, H.I. Smith, J. Vac. Sci. Technol. B **21**, 3112 (2003)
16. E.E. Moon, P.N. Everett, M.W. Meinhold, M.K. Mondol, H.I. Smith, J. Vac. Sci. Technol. B **17**, 2698 (1999)
17. P. Srisungsitthisunti, E.E. Moon, C. Tansarawiput, H. Zhang, M. Qi, X. Xu, Proc. SPIE **7767**, 776707 (2010)